PROTON-BEAM MACRO-PARTICLE INTERACTION: BEAM DUMPS AND QUENCHES

B. AUCHMANN, T. BAER, A. LECHNER, W. RIEGLER,
S. ROWAN, H. SCHINDLER, R. SCHMIDT, F. ZIMMERMANN

Abstract. We derive a model for the time evolution of beam losses due to macro particles falling into the LHC proton beam. The macro-particle initial longitudinal and transverse location, as well as its size are stochastic variables. By Monte-Carlo methods we determine the likelihood that beam-losses due to macro-particle/proton-beam interactions cause beam-dump triggers and/or quenches in beam-loss monitors and superconducting magnets, respectively.

Contents

Date: 4.12.2014.

1. Introduction

2. Beam-Charge Distribution

2.1. **2-D Gaussian Transverse Distribution.** As in [1, 2] we assume that the proton beam is continuous, i.e., we neglect the bunching of the beam, and we assume a Gaussian transverse beam profile. Note that in the rest frame of the protons, the distances between charges appear stretched by the Lorentz factor w.r.t. the same distance in the laboratory frame[1]. With $C = 26,659$ m, the LHC circumference in the laboratory frame, $N_\mathrm{p} = 2808 \cdot 1.3 \cdot 10^{11}$ the total number of protons in the beam, $e = 1.60 \cdot 10^{-19}$ C the elementary charge, and $\sigma_{x,y}$ the horizontal and vertical standard deviations, the charge density in the rest frame of the protons is

$$\tau'(x,y) = \frac{N_\mathrm{p} e}{\gamma C 2\pi\sigma_x\sigma_y} \mathrm{e}^{-\frac{x^2}{2\sigma_x^2}-\frac{y^2}{2\sigma_y^2}}. \tag{1}$$

The Lorentz factor is computed from the proton kinetic energy E_p by

$$\gamma = 1 + \frac{E_\mathrm{p}}{m_\mathrm{p} c^2}, \tag{2}$$

with $m_\mathrm{p} = 1.67 \cdot 10^{-27}$ kg the proton mass. For $E_\mathrm{p} = 6.5$ TeV$=e \cdot 6.5 \cdot 10^{12}$ J we find $\gamma = 6930.19$, whereas for 450 GeV we find $\gamma = 480.71$. The charge distribution in the laboratory frame is obtained by $\tau = \gamma\tau'$,

$$\tau(x,y) = \frac{N_\mathrm{p} e}{C 2\pi\sigma_x\sigma_y} \mathrm{e}^{-\frac{x^2}{2\sigma_x^2}-\frac{y^2}{2\sigma_y^2}}, \tag{3}$$

and the laboratory-frame current density $\vec{J} = J(x,y)\vec{\mathrm{e}}_\mathrm{s}$ is given by

$$J(x,y) = \frac{N_\mathrm{p} f e}{2\pi\sigma_x\sigma_y} \mathrm{e}^{-\frac{x^2}{2\sigma_x^2}-\frac{y^2}{2\sigma_y^2}}, \tag{4}$$

where, with v_p the proton velocity, $f = C v_\mathrm{p} \approx Cc = 11.25$ kHz.

2.2. **Beam parameters.** To determine the horizontal and vertical beam size, we obtain the beta function in the arc half-cell from the graphs in Fig. 1 and Eqs. (11.98) and (11.108) in [5]. The maximum of the beta function is given

$$\beta_\mathrm{max} = \frac{2L}{\sin\psi}\left(1 + \sin\frac{\psi}{2}\right), \tag{5}$$

[1] [3] uses the Lorentz transformation between standard inertial observers to derive the relation. That the same relations hold also for circular motion, where Lorentz transformation cannot be applied, is demonstrated in [4, Sec. 20].

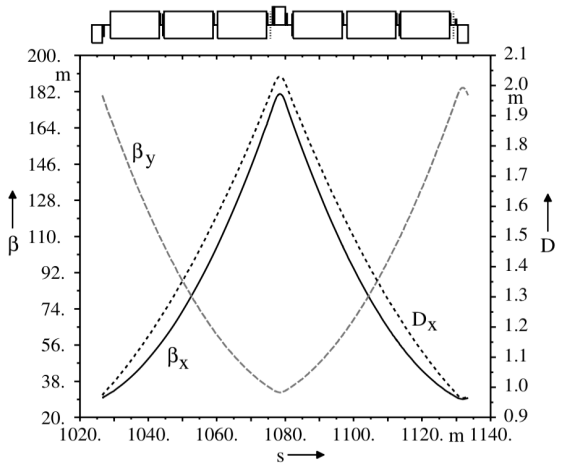

FIGURE 1. Beta functions and dispersion computed with MAD-X [7]. Picture reproduced from [5, Fig. 11.6].

where $\psi \approx \frac{\pi}{2}$ is the phase advance per cell in the LHC and $L = 53.45$ m is the half-cell length. With $b = \frac{1}{2}\sqrt{2L\beta_{\max} - L^2} - L$ we find a parabolic fit

$$\boxed{\beta_x(s) = \begin{cases} \frac{L}{2} + \frac{2(s+b)^2}{L}, & \text{if } s < L, \\ \frac{L}{2} + \frac{2(s-(b+2L))^2}{L}, & \text{if } s > L, \end{cases}} \tag{6}$$

$$\boxed{\beta_y(s) = \begin{cases} \frac{L}{2} + \frac{2(s-(b+L))^2}{L}, & \text{if } s < L, \\ \frac{L}{2} + \frac{2(s+(b-L))^2}{L}, & \text{if } s > L, \end{cases}} \tag{7}$$

where $s = 0$ m corresponds to the beginning of the half-cell, i.e., 1026 m in Fig. 1. The normalized emittance ϵ_{n} for Run 2 will be either 1.3 μm for BMCS beams, or 2.4 μm for nominal beams [6]. The final baseline has not been decided upon. An emittance blow-up of 20% and 5%, respectively, is to be expected at collisions. The geometric emittance is computed from the normalized emittance via

$$\boxed{\epsilon = \frac{\epsilon_{\mathrm{n}}}{\gamma\beta_{\mathrm{R}}} \sim \frac{\epsilon_{\mathrm{n}}}{\gamma},} \tag{8}$$

with $c = 299.79 \cdot 10^6$ m s^{-1} the vacuum speed of light and $\beta_{\mathrm{R}} = \frac{v_{\mathrm{p}}}{c}$. The horizontal and vertical beam sizes are given by

$$\boxed{\sigma_x(s) = \sqrt{\beta_x(s)\epsilon + \left(D(s)\frac{\Delta p}{p_0}\right)^2},} \tag{9}$$

$$\boxed{\sigma_y(s) = \sqrt{\beta_y(s)\epsilon}.} \tag{10}$$

3. Electric Field

3.1. **Beam Field.** To compute the electric field due to the proton beam, we map the electrostatic field $\vec{E}'_\mathrm{b}$ in the rest frame of the protons to the laboratory frame by Lorentz transformation[2]

$$\vec{E}_\mathrm{b} = \gamma \vec{E}'_\mathrm{b} \tag{11}$$

$$\vec{B}_\mathrm{b} = \frac{\gamma}{c^2} \vec{v}_\mathrm{p} \times \vec{E}'_\mathrm{b}. \tag{12}$$

The Lorentz factor in the charge density τ' is balanced by the same factor in the Lorentz transformation of the fields. We may, therefore, compute the transverse electric field in the laboratory frame as if the laboratory-frame charge distribution $\tau = \gamma\tau'$ was at rest, and we can compute the transverse magnetic field as if there was a stationary current density $\vec{J}$. The effect of the magnetic field on the transverse particle motion, however, is a second order effect and will be neglected.

The electric field of a 2-dimensional Gaussian charge distribution is described by the Bassetti-Erskine formula [9]. For $\sigma_x > \sigma_y$ we set

$$\sigma_0 = \sqrt{2(\sigma_x^2 - \sigma_y^2)}, \tag{13}$$

$$z_1 = \frac{1}{\sigma_0}\left(x\frac{\sigma_y}{\sigma_x} + \mathrm{i}y\frac{\sigma_x}{\sigma_y}\right), \tag{14}$$

$$z_2 = \frac{1}{\sigma_0}(x + \mathrm{i}y) \tag{15}$$

so that

$$z_1^2 - z_2^2 = -\frac{x^2}{2\sigma_x^2} - \frac{y^2}{2\sigma_y^2}, \tag{16}$$

and with $\varepsilon_0 = 8.85 \cdot 10^{-12}$ F m^{-1} the formula reads

$$\boxed{E_x = \frac{N_\mathrm{p} e}{2\varepsilon_0 C\sqrt{\pi}\sigma_0} \operatorname{Im}\left(w(z_2) - \mathrm{e}^{(z_1^2 - z_2^2)} w(z_1)\right),} \tag{17}$$

$$\boxed{E_y = \frac{N_\mathrm{p} e}{2\varepsilon_0 C\sqrt{\pi}\sigma_0} \operatorname{Re}\left(w(z_2) - \mathrm{e}^{(z_1^2 - z_2^2)} w(z_1)\right),} \tag{18}$$

where $w : \mathbb{C} \to \mathbb{C}$ is the complex generalization of the error function[3]

$$w(z) = \mathrm{e}^{-z^2}\left(1 + \frac{2\mathrm{i}}{\sqrt{\pi}}\int_0^z \mathrm{e}^{\zeta^2}\,\mathrm{d}\zeta\right). \tag{19}$$

See [10] for a detailed derivation. For symmetrically Gaussian beams, $\sigma_x = \sigma_y = \sigma$ the denominator in the leading factor and in the complex error function becomes zero,

[2]Note, there is no Lorentz transformation between a rotating fame as that of the rotating protons, and a standard-inertial frame as the laboratory frame. We neglect the rotation of the protons, which can be done on large enough scales, as explained in [8].

[3]In Mathematica, $w(z)$ can be computed by means of the $\mathrm{Erf}(z)$ function by $w(z) = \mathrm{e}^{-z^2}\big(1 - \mathrm{Erf}(-\mathrm{i}z)\big)$, using the numerical tricks shown in [11] and the function $\mathrm{Erfi}(z)$ which provides a stable implementation of $(1 - \mathrm{Erf}(z))$. For a stable Matlab implementation see [12].

leading to numerical instability in the implementation of the solution. We can use that, for large arguments, the complex error function has an asymptotic expansion [11]

$$w(z) \sim \frac{i}{\sqrt{\pi} z} \tag{20}$$

so that we find the expression for round beams

$$\boxed{E_x = -\frac{N_\mathrm{p} e}{2\pi\varepsilon_0 C}\mathrm{Im}\Big(\frac{1}{\mathrm{i}x - y}\Big)\Big(1 - \mathrm{e}^{-\frac{x^2+y^2}{2\sigma^2}}\Big),} \tag{21}$$

$$\boxed{E_y = -\frac{N_\mathrm{p} e}{2\pi\varepsilon_0 C}\mathrm{Re}\Big(\frac{1}{\mathrm{i}x - y}\Big)\Big(1 - \mathrm{e}^{-\frac{x^2+y^2}{2\sigma^2}}\Big),} \tag{22}$$

which gives[4] the familiar expression in polar coordinates

$$E_r = \frac{N_\mathrm{p} e}{2\pi\varepsilon_0 r C}\Big(1 - \mathrm{e}^{-\frac{r^2}{2\sigma^2}}\Big). \tag{23}$$

Finally, for $\sigma_y < \sigma_x$ we may use a simple coordinate transformation $y \mapsto x$ and $x \mapsto -y$ to find

$$\sigma_0 = \sqrt{2(\sigma_y^2 - \sigma_x^2)}, \tag{24}$$

$$z_1 = \frac{1}{\sigma_0}\left(y\frac{\sigma_x}{\sigma_y} + \mathrm{i}x\frac{\sigma_y}{\sigma_x}\right), \tag{25}$$

$$z_2 = \frac{1}{\sigma_0}(y + \mathrm{i}x) \tag{26}$$

so that

$$z_1^2 - z_2^2 = -\frac{x^2}{2\sigma_x^2} - \frac{y^2}{2\sigma_y^2} \tag{27}$$

and

$$\boxed{E_x = \frac{N_\mathrm{p} e}{2\varepsilon_0 C\sqrt{\pi}\sigma_0}\,\mathrm{Re}\left(w(z_2) - \mathrm{e}^{(z_1^2 - z_2^2)}w(z_1)\right),} \tag{28}$$

$$\boxed{E_y = \frac{N_\mathrm{p} e}{2\varepsilon_0 C\sqrt{\pi}\sigma_0}\,\mathrm{Im}\left(w(z_2) - \mathrm{e}^{(z_1^2 - z_2^2)}w(z_1)\right).} \tag{29}$$

3.2. **Mirror Charge Field.** We must also consider mirror charges of the macro-particle charge due to the beam-screen's highly-conductive copper liner. We consider that for macro-particles falling into the beam, the relevant contribution of mirror charges comes from the horizontal top and bottom surfaces of the beam screen. The electric field due to the mirror charge of the ionized macro particle is given by

$$\boxed{\vec{E}_\mathrm{m} = \frac{Qe}{16\pi\varepsilon_0 d_1^2}\vec{\mathrm{e}}_{n_1} + \frac{Qe}{16\pi\varepsilon_0 d_2^2}\vec{\mathrm{e}}_{n_2}} \tag{30}$$

where d_1 and d_2 denote the vertical distance of the particle from the upper and lower horizontal surfaces of the beam screen, i.e., $d_1 = h - y$ and $d_2 = 2h - d_1$ with $h =$

[4] To see this use $\frac{1}{\mathrm{i}x-y} = \frac{-\mathrm{i}x-y}{(\mathrm{i}x-y)(-\mathrm{i}x-y)} = \frac{-\mathrm{i}x-y}{r^2} = \frac{-\mathrm{i}r\cos(\varphi)-r\sin(\varphi)}{r^2}$.

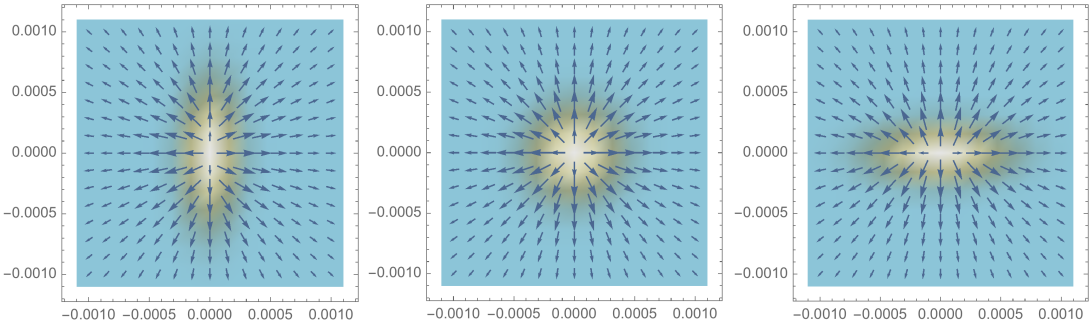

FIGURE 2. Electric field of the proton beam at three locations $s = 0, \frac{L}{2}, L$. The density plot represents the transverse charge density distribution Eq. (3). Axis coordinates are in meters.

$18.45 \cdot 10^{-3}$ m the half-height of the beam screen. $\vec{e}_{n_1}$ and $\vec{e}_{n_2}$ are the respective outward-pointing normal vectors. Mirror charges are mostly relevant when the particle is close to the beam-screen surface. The initial-position of the macro-particle is at $y = h - R$ for the top surface, and $y = -(h - R)$ for the bottom surface, where R is the macro-particle radius. Above, we included also the distant surface so that the equation is valid for both, particles falling into the beam, and particles lifted up from the bottom surface. Note that in [1] a round beam tube was assumed for the calculation of mirror fields. We neglect mirror charges of the beam charge distribution, as well as screening currents in the beam screen.

4. Equation of Motion

The equation of motion of the macro particle is given by

$$\ddot{\vec{r}} = \left(\frac{Qe}{m} \left(\vec{E} + \dot{\vec{r}} \times \vec{B} \right) + \vec{g} \right), \tag{31}$$

where $\ddot{\vec{r}} = \vec{a}$ is the acceleration, m is the macro-particle's mass, $\dot{\vec{r}} = \vec{v}$ is the macro-particle velocity, and $\vec{g} = -g\vec{e}_y$, with $\vec{e}_y$ the vertical direction and $g = 9.81$ ms^{-2} the gravitational constant. With the above results, the equation of motion of the particle, relevant for the simulation of UFO events, is given by

$$\boxed{\vec{a} = \left(\frac{3Qe}{4\pi R^3 \rho} \left(\vec{E}_{\mathrm{b}} + \vec{E}_{\mathrm{m}} \right) + \vec{g} \right),} \tag{32}$$

where ρ is its density. Q denotes the macro-particle charge expressed in numbers of electron charges e, and m denotes the particle mass.

5. Charging Rate of the Macro Particle

5.1. **Knock-On Electron Probability.** [13, Sec. III.14, p. 71] gives the charging rate $\dot{Q}$ of the macro particle that moves into the proton beam. The starting point for

the charging rate is the distribution of secondary electrons, related to the Bethe-Bloch formula [13] and expressed in SI units following [14]

$$\frac{\partial^2 N}{\partial T \partial s} = 2\pi r_\mathrm{e}^2 m_\mathrm{e} c^2 z^2 n \frac{1}{\beta_\mathrm{R}^2} \frac{F(T)}{T^2} \tag{33}$$

with the electron density in the macro particle

$$n = \frac{N_\mathrm{A} Z \rho}{A M_\mathrm{u}}, \tag{34}$$

and the classical electron radius

$$r_\mathrm{e} = e^2/(4\pi\varepsilon_0 m_\mathrm{e} c^2), \tag{35}$$

$r_\mathrm{e} = 2.82 \cdot 10^{-15}$ m. N is the number of secondary electrons at a kinetic energy T, s is the distance into the macro particle, $N_\mathrm{A} = 6.02 \cdot 10^{23}$ mol^{-1} the Avogadro number, $m_\mathrm{e} = 9.11 \cdot 10^{-31}$ kg the electron mass, ze the charge of the incident particle ($z = -1$ for protons), Z the atomic number, A the relative atomic mass, $M_\mathrm{u} = 10^{-3}$ kg mol^{-1} the molar mass constant, and, finally, $F(T)$ is a spin-dependent factor [15, p. 14–16] that reads for protons

$$F(T) = 1 - \beta_\mathrm{R}^2 \frac{T}{T_\mathrm{max}} + \frac{1}{2}\left(\frac{T}{E_\mathrm{p} + m_\mathrm{p} c^2}\right)^2. \tag{36}$$

T_max is the maximum energy that can be transferred to the electron

$$T_\mathrm{max} = \frac{2 m_\mathrm{e} c^2 \beta_\mathrm{R}^2 \gamma^2}{1 + 2\gamma \frac{m_\mathrm{e}}{m_\mathrm{p}} + \left(\frac{m_\mathrm{e}}{m_\mathrm{p}}\right)^2}, \tag{37}$$

which results for $\beta_\mathrm{R} \to 1$ and $\gamma = 7500$ (LHC protons at 7 TeV) in $T_\mathrm{max} = 6.25$ TeV $\approx E_\mathrm{p}$. We find

$$\frac{\partial^2 N}{\partial T \partial s} \approx \frac{\pi N_\mathrm{A} r_\mathrm{e}^2 m_\mathrm{e} c^2 \rho}{M_\mathrm{u} T^2} \left(1 - \frac{T}{T_\mathrm{max}} + \frac{1}{2}\frac{T^2}{E_\mathrm{p}^2}\right), \tag{38}$$

where we used $Z/A \approx 1/2$ and $E_\mathrm{p} + m_\mathrm{p} c^2 = E_\mathrm{p}(1 + \frac{1}{\gamma}) \approx E_\mathrm{p}$ and $\beta_\mathrm{R} \approx 1$.

5.2. **Minimum Energy Transfer for Ionization.** We can write the charging rate of the macro particle as

$$\dot{Q} = \int_{\mathscr{A}} \int_{\mathscr{S}} \int_{T_\mathrm{min}}^{T_\mathrm{max}} J(x, y) \frac{\partial^2 N}{\partial T \partial s} \, \mathrm{d}T \, \mathrm{d}s \, \mathrm{d}a, \tag{39}$$

i.e., $\dot{Q}$ is the number of elementary charges per unit time that the macro particle accumulates. $\mathscr{A}$ is the cross-sectional area of the macro-particle, facing the proton beam. Note that the location of $\mathscr{A}$ w.r.t. to the beam center is a function of time as the particle moves into the beam. $\mathscr{S}$ is the path that an incident proton takes through the macro particle.

The minimum energy $T_{\min}$ for the ionization of an atom is given in [13] by the ionization constant[5]

$$I = 16\ \mathrm{eV} \cdot Z^{0.9} \tag{40}$$

For the electron to leave the macro-particle, however, it has to traverse the macro particle, and overcome the Coulomb potential ϕ

$$\phi(Q) = \frac{Qe^2}{4\pi\varepsilon_0 R}. \tag{41}$$

Electrons that just make it out of the macro particle are emitted almost perpendicular to the proton track [16, p. 7]. The practical range r is given by the empirical relation

$$r(T) = \frac{AT}{\rho}\left(1 - \frac{B}{1+CT}\right), \tag{42}$$

where $A = \frac{5.37\cdot 10^{-6}}{e}\ \mathrm{kg\,m^{-2}\,J^{-1}}$, $B = 0.9815$, and $C = \frac{3.123\cdot 10^{-6}}{e}\mathrm{J^{-1}}$. To determine the minimum energy to escape from the macro particle, we need to determine the average path length L that an electron, emanating from any location inside the macro-particle sphere, has to traverse in the transverse plane to the proton track. Let the electron be kicked at a longitudinal coordinate y defined w.r.t. to the sphere's central transverse plane. The transverse section of the sphere at y is a circle of radius $\bar{R}(R, y) = \sqrt{R^2 - y^2}$. For a given radial offset d of the incident proton from the central longitudinal axis of the macro particle, an electron path, averaged over the all azimuthal angles θ, has the length L''

$$L''(R, d, y) = \frac{1}{2\pi}\int_0^{2\pi} d\cos\theta + \sqrt{d^2\cos^2\theta + \bar{R}^2(R, y) - d^2}\,\mathrm{d}\theta. \tag{43}$$

The full length of the proton path through the macro particle is $g(R, d) = 2\sqrt{R^2 - d^2}$ and the average of electron path lengths over the proton path is given by

$$L'(R, d) = \frac{1}{g(R, d)}\int_{-\frac{g}{2}}^{\frac{g}{2}} L''(R, d, y)\,\mathrm{d}y. \tag{44}$$

Finally, the average over all transverse locations (d, φ) of the proton path yields the average electron path length

$$L(R) = \frac{1}{R^2\pi}\int_0^R\int_0^{2\pi} L'(R, d)d\,\mathrm{d}d\mathrm{d}\varphi. \tag{45}$$

Numerical integration yields $L(R) = 0.7358R$. The above range equation can be inverted, and we obtain the minimum energy for a range equal to the average path length $L(R)$ of

$$T(R) = \frac{A(B-1) + CL(R)\rho + \sqrt{4ACL(R)\rho + (A(B-1) + CL(R)\rho)^2}}{2AC}. \tag{46}$$

Finally, the minimum energy that needs to be, on average, transferred to an electron to leave the macro particle is

$$T_{\min}(Q, R) = \varphi(Q) + T(R). \tag{47}$$

[5] In [14] we find $I = 10\ \mathrm{eV} \cdot Z$.

5.3. **Charging Rate.** For macro-particles that are small w.r.t. the beam size, $R \ll \sigma$, the integral Eq. (39) can be rewritten in three factors

$$\dot{Q} = \int_{\mathscr{A}} J(x,y)\,\mathrm{d}a \int_{\mathscr{S}} \mathrm{d}s \int_{T_{\min}}^{T_{\max}} \frac{\partial^2 N}{\partial T \partial s}\,\mathrm{d}T. \tag{48}$$

We find

$$\int_{\mathscr{A}} J(x,y)\,\mathrm{d}a = R^2\pi J(x,y) = \frac{N_\mathrm{p} f R^2}{2\sigma_x\sigma_y} \mathrm{e}^{-\frac{x^2}{2\sigma_x^2}-\frac{y^2}{2\sigma_y^2}}, \tag{49}$$

where (x,y) are the coordinates of the center of the macro particle w.r.t. the beam center. The average length S of a path through the macro particle is given by

$$\begin{aligned} S &= \frac{1}{R^2\pi}\int_0^{2\pi}\int_0^R 2\sqrt{R^2-r^2}\,r\,\mathrm{d}r\mathrm{d}\varphi \\ &= \frac{4R}{3}, \end{aligned} \tag{50}$$

so that

$$\int_{\mathscr{S}} \mathrm{d}s \approx S = \frac{4R}{3}. \tag{51}$$

$T_{\min}$ is of the order of several tens of keV, so that $T_{\max} \gg T_{\min}$ and the upper integrand may be set to ∞. Moreover, the impact of $F(T)$ on this integral is negligible, so that we can set $F(T) \approx 1$. It follows that

$$\begin{aligned} \int_{T_{\min}}^{T_{\max}} \frac{\partial^2 N}{\partial T\partial s}\,\mathrm{d}T &\approx \int_{T_{\min}}^{\infty} \frac{\partial^2 N}{\partial T\partial s}\,\mathrm{d}T \\ &= \frac{\pi N_\mathrm{A} r_\mathrm{e}^2 m_\mathrm{e} c^2 \rho}{T_{\min} M_\mathrm{u}}. \end{aligned} \tag{52}$$

The product finally reads

$$\boxed{\dot{Q} = \frac{2N_\mathrm{p} f R^3 \pi N_\mathrm{A} r_\mathrm{e}^2 m_\mathrm{e} c^2 \rho}{3\sigma_x\sigma_y T_{\min}(Q,R) M_\mathrm{u}}\,\mathrm{e}^{-\frac{x^2}{2\sigma_x^2}-\frac{y^2}{2\sigma_y^2}}.} \tag{53}$$

Note that this differs from the formula given in [1] where $T_{\min}$ equals the Coulomb potential.

As a cross-check, we simulate the ionization of a spherical Si particle by incident high-energy protons with the Garfield++ software [17]. In the simulation the sphere is bombarded by 10^5 protons, evenly distributed over the cross-sectional area of the sphere. The average charge produced per proton Q_pp is compared to the formula

$$Q_\mathrm{pp}(R) = \frac{\dot{Q}}{\int_{\mathscr{A}} J(x,y)\,\mathrm{d}a} = \frac{4\pi R N_\mathrm{A} r_\mathrm{e}^2 m_\mathrm{e} c^2 \rho}{3\,T_{\min}(Q,R)\,M_\mathrm{u}}, \tag{54}$$

where the initial macro-particle charge Q is set to zero. Results are shown in Fig. 3. Analytical model and numerical simulation agree to within 30-40% w.r.t. the simulated curve.

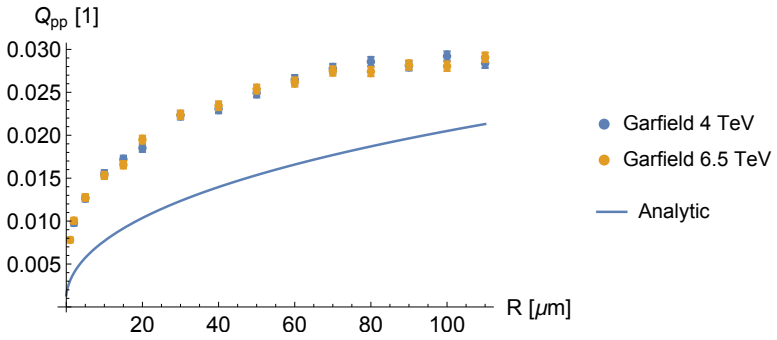

FIGURE 3. Average ionization charge Q_{pp} (in units of electron charge) produced by an incident high-energy proton in an initially electrically neutral Si sphere of radius R. Garfield++ [17] simulations are compared to Eq. (54).

6. Rate of Inelastic Interactions

We can estimate the rate of inelastic interactions between the atomic nulcei in the macro particle and the proton beam. For this, we give the interaction cross-sections, which can be estimated by [18]

$$\sigma_{\mathrm{iel}} = \pi r_0^2 A^{\frac{2}{3}}, \tag{55}$$

where $r_0 = 1.2 - 1.5$ fm is an empirical constant [19]. The cross-section is typically expressed in mbarn, where 1 barn $= 1.0 \cdot 10^{-28}$ m^2. More accurate cross-sections computed with FLUKA [20, 21] are given in Tab. 2

The macroscopic section is given by

$$\Sigma_{\mathrm{iel}} = \sigma_{\mathrm{iel}} \rho_A, \tag{56}$$

where

$$\rho_A = \frac{N_{\mathrm{A}} \rho}{A M_{\mathrm{u}}}, \tag{57}$$

is the atom density. The negative rate of inelastic interactions equals the proton loss rate $\dot{N}_{\mathrm{p}}$, which is given by

$$\boxed{\dot{N}_{\mathrm{p}} = -\int_{\mathscr{A}} \int_{\mathscr{S}} J(x,y) \Sigma_{\mathrm{iel}} \, \mathrm{d}s \, \mathrm{d}a = -\frac{2 N_{\mathrm{p}} f \sigma_{\mathrm{iel}} R^3 N_{\mathrm{A}} \rho}{3 \sigma_x \sigma_y A M_{\mathrm{u}}} \mathrm{e}^{-\frac{x^2}{2\sigma_x^2} - \frac{y^2}{2\sigma_y^2}}.} \tag{58}$$

The beam life-time can be estimated as

$$\tau_{\mathrm{b}} = -\frac{N_{\mathrm{p}}}{\dot{N}_{\mathrm{p}}}. \tag{59}$$

This treatment neglects that protons may be lost into collimators due to single-diffractive or elastic interactions, as well as other effects.

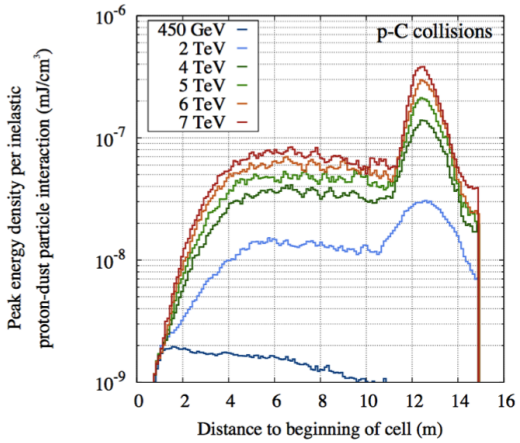

FIGURE 4. Peak energy deposition in MB coil per proton-C-atom interaction for different beam energies. The characteristic peak downstream towards the end of the magnet is due to neutral particles hitting the down-stream beam pipe because of the slight curvature of the MB magnets.

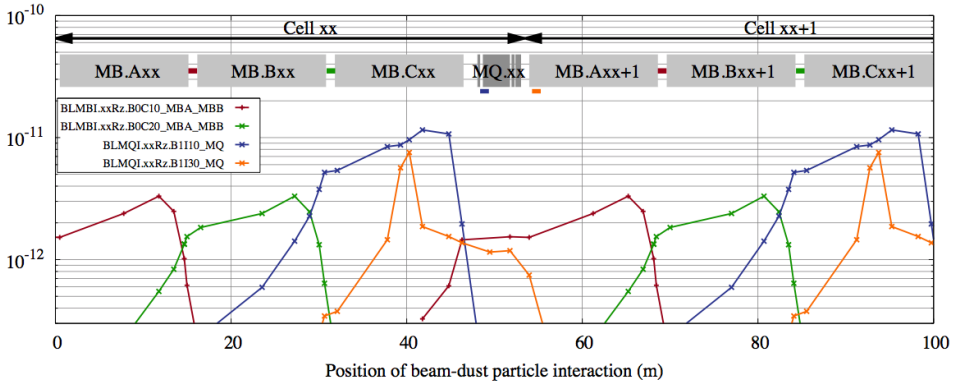

FIGURE 5. BLM signal in Gy per proton-C-atom interaction in the in the four BLM locations in an arc cell. The signals are plotted as a function of UFO location.

7. BLM Signals and Thresholds

A FLUKA model [22] predicts the energy deposition in the superconducting coils per inelastic proton-atom interaction in the beam center (see Fig. 4) as a function of beam energy. Moreover, the FLUKA model provides the respective BLM response as a function of longitudinal loss location and energy (see Fig. 5).

The data recorded in the different runnings sums (RS) of a BLM is calculated for a respective integration time t_{int}, at an energy-level E_{p}, and for an interaction at the

longitudinal location s by

$$\boxed{\mathrm{BLMSignal}(t,s) = -\dot{N}_\mathrm{p}(\vec{r}(t)) \cdot \mathrm{BLMResponse}(E_\mathrm{p},s),} \tag{60}$$

$$\boxed{\mathrm{RS}(t_\mathrm{int},t,s) = \int_{t-t_\mathrm{int}}^{t} \mathrm{BLMSignal}(t,s)\,\mathrm{d}t,} \tag{61}$$

where $\dot{N}_\mathrm{p}(t)$ is the rate of inelastic interactions between the macro-particle and the beam derived above.

Electro-thermal models allow to estimate whether a given energy deposition in a superconducting coil as a function of space and time would generate a quench. The so-called RS-at-quench is computed by

$$\boxed{\mathrm{RS@Quench}(E_\mathrm{p},t_\mathrm{int},s) = \frac{\mathrm{BLMResponse}(E_\mathrm{p},s)\cdot\mathrm{QuenchLevel}(E_\mathrm{p},t_\mathrm{int})}{\mathrm{EnergyDeposit}(E_\mathrm{p})}.} \tag{62}$$

For the electro-thermal estimate of $\mathrm{QuenchLevel}(E_\mathrm{p},t_\mathrm{int})$ a constant power pulse in time with the spatial distribution from FLUKA is assumed. Note that this may not correspond precisely to the quench level due to the rising flank of a roughly Gaussian-shaped UFO beam loss. The error due to this effect is estimated to be within 20%.

When setting the BLM thresholds in the arcs, the longitudinal loss-location is not known. The threshold is, therefore, computed using the minimal BLM response within the longitudinal range where the respective BLM shows a larger signal than all others.[6] We call this value $\mathrm{MinBLMResponse}(E_\mathrm{p})$. The BLM threshold is computed by

$$\boxed{\mathrm{BLMThreshold}(E_\mathrm{p},t_\mathrm{int}) = \frac{\mathrm{MinBLMResponse}(E_\mathrm{p})\cdot\mathrm{QuenchLevel}(E_\mathrm{p},t_\mathrm{int})}{\mathrm{EnergyDeposit}(E_\mathrm{p})}.} \tag{63}$$

The $\mathrm{BLMThreshold}(E_\mathrm{p},t_\mathrm{int})$ is computed for 12 time ranges between 40 μs to 82 s, and for 32 energy levels to produce the full thresholds table. A BLM-induced beam dump will occur whenever

$$\mathrm{RS}(t_\mathrm{int},t,s) > \mathrm{BLMThreshold}(E_\mathrm{p},t_\mathrm{int}) \quad \text{for any } t_\mathrm{int}. \tag{64}$$

8. Monte Carlo Model

We want to estimate the likelihood for a UFO event to cause a beam dump. The model stretches over the basic repetitive element of the arc that is the cell. We implement a UFO generator based on three distributions. The longitudinal distribution is constant

$$D_s(s) = \frac{1\ \mathrm{m}}{2L} \tag{65}$$

[6] It follows that the orange BLM response in Fig. 5 is not used to protect rom UFO-induced quenches.

with $L = 53.45$ m the half-cell length. The transverse distribution is equally constant for $x \in [0, x_{\max}$ [7]

$$D_x(x) = \frac{1\text{ m}}{x_{\max}} \tag{66}$$

with $x_{\max} < 14.15 \cdot 10^{-3}$ m the half-width of the beam-screen upper and lower planes. To make the model efficient, we should narrow down $x_{\max}$ to the stretch of the beam screen that produces measurable peaks[8] in the BLM signals. Due to symmetry, we need not consider negative x-values.

The third distribution needed to start a Monte-Carlo simulation is the volume of the macro particle. Based on dust observations in CERN buildings SMI2 and 113 cited in [23, Fig. 5.4(b)] dust particle volumes range from 0.5 μm^3 to $3 \cdot 10^4$ μm^3] (corresponding, for spherical macro particles to a range of radis R between 0.5 μm and 25 μm) with a distribution $\propto \left(\frac{1\text{ m}^3}{V}\right)^2$. We, therefore, propose a normalized distribution function for $V \in [V_{\min}, V_{\max}]$

$$D_V(V) = \frac{V_{\max} V_{\min}}{V_{\max} - V_{\min}} \frac{1\text{ m}^3}{V^2}, \tag{67}$$

where, as in the case of the x-distribution above, the upper and lower limits should be chosen such that only relevant UFO events are considered.

Algorithm 1 illustrates how a series of UFO events can be simulated with stochastic input data for initial macro-particle location and size. The functionality of the code is further increased by mimicking the UFO Buster application's analysis features, as shown in Algorithm 2. The implementation of the algorithms should make use of parallel computing.

9. Results

9.1. **Pre-LS1.**

9.2. **Post-LS1.**

9.3. **Large-Emittance Bunches.** [23] cites the idea to inject a few bunches with increased emittance that, while not appreciably reducing luminosity, fend off falling macro-particles before they could reach the high-power core of the beam. The above algorithm is well suited to simulate this type of setup, requiring, in a first approximation, only a superposition of two beams, one with $N_{\text{p}1} = (N_{\text{b}} - N_\ell) \cdot I_{\text{b}}$ and normal emittance, and one with $N_{\text{p}}2 = N_\ell \cdot I_{\text{b}}$ and large emittance, N_ℓ denoting the number of large-emittance bunches and I_{b} the bunch intensity.

[7] Maybe it would be worth to study accumulations of UFOs under the pumping slots of the beam screen?

[8] According to [23, Sec. 5.1.1] a UFO is detectable by the UFO Buster application if it leads to a signal larger or equal to 10^{-4} Gy in the 640 μs running sum of at least two BLMs within 40 m.

Algorithm 1 Monte Carlo algorithm to study UFO events in the LHC

Select E_p, ε_n, top or bottom location, macro-particle material, N_MC, Δt
Initialize N_u, N_d, N_f, $N_\mathrm{q} = 0$
for $i = 1 \dots N_\mathrm{MC}$ **do**
  Generate s, x_0, and V from D_s, D_x, and D_V, respectively (65),(66),(67)
  Compute $\sigma_x(s)$, $\sigma_y(s)$, $R = \left(\frac{3V}{4\pi}\right)^{\frac{1}{3}}$, and $y_0 = \pm(h - R)$ (6),(8),(9)
  Initialize $j = 0$, $t_0 = 0$, $\vec{r}_0 = x_0\vec{e}_x + y_0\vec{e_y}$, $\vec{v}_0 = \vec{0}$, $Q_0 = 0$, $N_\mathrm{p0} = 0$
  repeat
    $j = j + 1$
    $t_j = t_{j-1} + \Delta t$
    $\vec{r}_j = \vec{r}_{j-1} + \Delta t\ \vec{v}_{j-1}$
    $\vec{v}_j = \vec{v}_{j-1} + \Delta t\ \vec{a}(\vec{r}_{j-1}, Q_{j-1})$ (17),(21),(28),(30),(32)
    $Q_j = Q_{j-1} + \Delta t\ \dot{Q}(\vec{r}_{j-1}, N_\mathrm{p}{j-1})$ (53)
    $N_\mathrm{p}{j} = N_\mathrm{p}{j-1} + \Delta t\ \dot{N}_\mathrm{p}(\vec{r}_{j-1}, N_\mathrm{p}{j-1})$ (58)
  until $|\vec{r}_j| > |\vec{r}_{j-1}|$ **and** $\forall$BLMs : BLMSignal$(t_j, s) < 0.1$ Gy/s (60)
  Call **UFOBuster**$(\dot{N}_\mathrm{iel}(t), N_\mathrm{u}, N_\mathrm{d}, N_\mathrm{f}, N_\mathrm{q})$ Alg. 2
end for

10. Summary

Appendix A. Constants and Parameters

Constants and LHC parameters are summarized in Tab. 1. Relevant material parameters for the macro particle are given in Tab. 2.

Table 1. Constants used throughout this note.

Symbol	Value	Name
N_p	$2808 \cdot 1.3 \cdot 10^{11}$	Post-LS1 nominal number of protons
e	$1.60 \cdot 10^{-19}$ C	Electron charge
C	$26,659$ m	LHC circumference
m_p	$1.67 \cdot 10^{-27}$ kg	Proton rest mass
c	$299.79 \cdot 10^{6}$ m s^{-1}	Vacuum speed of light
f	11.25 kHz	LHC revolution frequency
L	53.45 m	Half-cell length
ϵ_n	1.3 μm	Normalized emittance BMCS beam
ϵ_n	2.4 μm	Normalized emittance nominal beam
ε_0	$8.85 \cdot 10^{-12}$ F m^{-1}	Vacuum electrical permittivity
h	$18.45 \cdot 10^{-3}$ m	Beam screen height
g	9.81 m s^{-2}	Gravitational constant
r_e	$2.82 \cdot 10^{-15}$ m	Classical electron radius
m_e	$9.11 \cdot 10^{-31}$ kg	Proton rest mass
N_A	$6.02 \cdot 10^{23}$ mol^{-1}	Avogadro Number
M_u	$1.0 \cdot 10^{-3}$ kg mol^{-1}	Molar mass constant

Algorithm 2 UFO Buster analysis

Initialize $B_\mathrm{u}=0$, $B_\mathrm{d}=0$, $B_\mathrm{f}=0$, B_q=0*Booleans for detection of various UFO types*
for All BLMs $k=1\ldots6$ **do**
  if $\max\left(\mathrm{RS}(640\ \mu\mathrm{s},t,s)\right)/640\ \mu\mathrm{s} > 0.1$ Gy/s **then**
    $B_\mathrm{u}=1$ *Registered as UFO*
    for all RS $\ell=1\ldots12$ **do**
      if $\max\left(\mathrm{RS}(t_\mathrm{int},t,s)\right) > \mathrm{BLMThreshold}(E_\mathrm{p},t_\mathrm{int})$ **then**
        $B_\mathrm{d}=1$ (61)(63) *Beam-dumping UFO*
        if $\max\left(\mathrm{RS}(t_\mathrm{int},t,s)\right) < \mathrm{RS@Quench}(E_\mathrm{p},t_\mathrm{int},s)$ **then**
          $B_\mathrm{f}=1$ (62) *Avoidable beam-dump*
        else
          if $t_\mathrm{int}+\mathrm{TimeToDump} < \mathrm{MPSResponseTime}$ **then**
            $B_\mathrm{q}=1$ *Quench despite beam dump*
          end if
        end if
      end if
    end for
  end if
end for
$N_\mathrm{u}=N_\mathrm{u}+B_\mathrm{u}$ *Number of UFOs*
$N_\mathrm{d}=N_\mathrm{d}+B_\mathrm{d}$ *Number of beam dumps*
$N_\mathrm{f}=N_\mathrm{f}+B_\mathrm{f}$ *Number of avoidable beam dumps*
$N_\mathrm{q}=N_\mathrm{q}+B_\mathrm{q}$ *Number of unavoidable quenches*
Fit Gaussians to rising and falling edge of BLMSignal
Record σ_rise and σ_fall

TABLE 2. FLUKA cross-sections for inelastic collisions of 6.5 TeV-protons with the macro-particle, as well as the elements' atomic numbers, atomic masses, and mass densities.

Material	σ_iel [mbarn]	Z	A	ρ [kg m^{-3}]
Carbon	266[9]	6	12.01	2250
Copper	850	29	63.55	8960
Aluminum	470	13	26.98	2700
Silicon	530[10]	14	2809	2328

APPENDIX B. POST-LS1 THRESHOLDS

B.1. **BLM Response.** Tables 3-5 give numerical values of the BLMResponse function at 7 TeV. To obtain data at 4 TeV, it is suggested to scale the results linearly with energy [24].

[10]To check the energy-dependence of the cross-sections a FLUKA calculation at 450 GeV gave 245 mbarn.
[11]From Eq. (55).

TABLE 3. BLMResponse at 7 TeV in the BLMBI.xxRz.B0C10_MBA_MBB, the BLM vertically above MB.A-MB.B interconnect and the red line in Fig. 5.

Position [m]	Value [Gy/s]	Statistical Error [%]
-11.654	$3.2695 \cdot 10^{13}$	10.7
-8.65472	$6.0905 \cdot 10^{13}$	6.9
-7.153	$1.4525 \cdot 10^{12}$	4.9
-1.68889	$1.5393 \cdot 10^{12}$	4.2
0.496244	$1.5218 \cdot 10^{12}$	4.1
7.77869	$2.3873 \cdot 10^{12}$	2.9
11.7781	$3.3090 \cdot 10^{12}$	2.4
13.4778	$2.4828 \cdot 10^{12}$	3.8
14.6776	$1.0163 \cdot 10^{12}$	5.9
14.9797	$6.1615 \cdot 10^{13}$	5.6
16.5391	$1.5323 \cdot 10^{13}$	15.5

TABLE 4. BLMResponse at 7 TeV in the BLMBI.xxRz.B0C20_MBA_MBB, the BLM vertically above MB.B-MB.C interconnect and the green line in Fig. 5.

Position [m]	Value [Gy/s]	Statistical Error [%]
7.77869	$2.2428 \cdot 10^{13}$	10.5
11.7781	$5.4843 \cdot 10^{13}$	6.4
13.4778	$8.3447 \cdot 10^{13}$	5.6
14.0777	$1.3343 \cdot 10^{12}$	4.3
14.6776	$1.3439 \cdot 10^{12}$	5.0
14.9797	$1.5428 \cdot 10^{12}$	3.2
16.5391	$1.8319 \cdot 10^{12}$	4.6
23.538	$2.3873 \cdot 10^{12}$	2.9
27.2373	$3.3090 \cdot 10^{12}$	2.4
28.937	$2.4653 \cdot 10^{12}$	4.6
30.0367	$1.3246 \cdot 10^{12}$	3.3
30.6387	$6.3963 \cdot 10^{13}$	6.1
32.0982	$1.3369 \cdot 10^{13}$	18.2

B.2. **Energy Deposit.** The peak energy deposit in an MB coil due to a proton-Carbon-atom collision is $1.35 \cdot 10^{-7}$ mJ cm^{-3} at 4 TeV, and $3.29 \cdot 10^{-7}$ mJ cm^{-3} at 6.5 TeV; compare with Fig. 4.

B.3. **Quench Level.** In Tab. 6, quench levels are given in mJ cm^{-3}. for two beam-energy levels. 3.93 TeV is the setting used in BLMs at 4 TeV beam energy, and the 6.39 TeV setting is used at 6.5 TeV.

TABLE 5. BLMResponse at 7 TeV in the BLMQI.xxRz.B1I10_MQ, the BLM vertically above MB.C-MQ interconnect and the blue line in Fig. 5.

Position [m]	Value [Gy/s]	Statistical Error [%]
0.496244	$1.2405 \cdot 10^{13}$	19.6
7.77869	$1.2230 \cdot 10^{13}$	17.5
11.7781	$1.5778 \cdot 10^{13}$	18.3
13.4778	$1.8958 \cdot 10^{13}$	19.1
14.0777	$2.5100 \cdot 10^{13}$	14.7
14.6776	$2.8236 \cdot 10^{13}$	15.3
14.9797	$2.7947 \cdot 10^{13}$	16.8
16.5391	$2.3435 \cdot 10^{13}$	22.7
23.538	$5.9284 \cdot 10^{13}$	9.9
27.2373	$1.4152 \cdot 10^{12}$	7.2
28.937	$2.2690 \cdot 10^{12}$	5.2
30.0367	$3.7636 \cdot 10^{12}$	2.9
30.6387	$5.1820 \cdot 10^{12}$	2.6
32.0982	$5.3818 \cdot 10^{12}$	2.5
37.797	$8.4270 \cdot 10^{12}$	5.2
39.2966	$8.6977 \cdot 10^{12}$	2.1
40.2964	$9.6018 \cdot 10^{12}$	3.1
41.796	$1.1556 \cdot 10^{11}$	2.3
44.7953	$1.0706 \cdot 10^{11}$	1.6
46.297	$1.9615 \cdot 10^{12}$	5.6
49.4613	$4.8903 \cdot 10^{14}$	28.4

TABLE 6. Minimum energy-density to quench (quench level) in MB coils on the inner-layer midplane turn for twelve running sums and two energy levels. Energy levels are given in TeV, integration times in seconds, and quench levels in $\mathrm{mJ\,cm^{-3}}$.

E_p / t_int	$40 \cdot 10^{-6}$	$80 \cdot 10^{-6}$	$320 \cdot 10^{-6}$	$640 \cdot 10^{-6}$	$2.56 \cdot 10^{-3}$	$10.24 \cdot 10^{-3}$
3.93	14.55	14.94	18.38	21.61	29.1	46.93
6.39	4.58	4.75	5.93	7.97	12.81	21.11
E_p / t_int	$81.92 \cdot 10^{-3}$	0.66	1.31	5.24	20.97	83.89
3.93	127.22	381.43	505.43	1,003.10	3,161.89	12,478.59
6.39	57.81	153.54	210.96	509.76	1,866.32	7,437.21

APPENDIX C. PRE-LS1 BLM THRESHOLDS

In Tab. 7 we give the BLM thresholds in the three pre-LS1 BLM locations on the MQ magnets. Note that the thresholds were set a factor three lower than the assumed quench level.

TABLE 7. Pre-LS1 thresholds at $E_\mathrm{p} = 3.93$ TeV (settings used for 4 TeV operation) for three BLM positions and twelve integration times. Thresholds are given in mGy and integration times are given in seconds.

Pos. / t_int	$40 \cdot 10^{-6}$	$80 \cdot 10^{-6}$	$320 \cdot 10^{-6}$	$640 \cdot 10^{-6}$	$2.56 \cdot 10^{-3}$	$10.24 \cdot 10^{-3}$
1	0.07	0.13	0.31	0.31	0.31	0.31
2	0.05	0.09	0.21	0.21	0.21	0.21
3	0.05	0.09	0.21	0.21	0.21	0.21
Pos. / t_int	$81.92 \cdot 10^{-3}$	0.66	1.31	5.24	20.97	83.89
1	0.65	1.84	1.97	2.62	6.29	16.78
2	0.44	2.49	2.75	3.67	8.39	25.17
3	0.44	2.49	2.75	3.67	8.39	25.17

REFERENCES

[1] F. Zimmermann, M. Giovannozzi, and A. Xagkoni. Interaction of macro-particles with LHC proton beam. *Proceedings of IPAC 2010, Kyoto, Japan*, (MOPEC016):492–494, 2010.

[2] F. Zimmermann. Trapped dust in HERA and DORIS. DESY HERA 93-08, DESY, Hamburg, Germany, July 1993.

[3] http://en.wikipedia.org/wiki/Length_contraction#Moving_length_is_known. Last checked November 2014.

[4] B. Auchmann and S. Kurz. Observers and splitting structures in relativistic electrodynamics. *J. Phys. A: Math. Theor.*, 47(435202), 2014.

[5] S. Russenschuck. *Field Computation for Accelerator Magnets: Analytical and Numerical Methods for Electromagnetic Design and Optimization*. Wiley-VCH, first edition, March 2010.

[6] R. Bruce, G. Arduini, S. Fartoukh, M. Giovannozzi, M. Lamont, E. Metral, T. Pieloni, S. Redaelli, and J. Wenninger. Baseline LHC machine parameters and configuration of the 2015 proton run. *Proceedings of the 2014 LHC Performance Workshop, Chamonix, France*, 2014.

[7] W. Herr, F. Schmidt, "A MAD-X Primer", CERN AB Note, CERN-AB-2004-027-ABP, 2004.

[8] B. Mashhoon. The hypothesis of locality in relativistic physics. *Physics Letters A*, 145(4):147–153, April 1990.

[9] M. Bassetti and G. A. Erskine. Closed expression for the electrical field of a two-dimensional gaussian charge. Technical Note CERN-ISR-TH/80-06, CERN, Geneva, Switzerland, March 1980.

[10] R. Wanzenberg. Nonlinear motion of a point charge in the 3d space charge field of a Gaussian bunch. Internal Report DESY M 10-01, DESY, May 2010.

[11] V. Ziemann. Beyond Bassetti and Erskine: Beam-beam deflections for non-Gaussian beams. Project Note SLAC-PUB-5582, SLAC, Stanford CA 94309, June 1991.

[12] J. A. C. Weideman. Computation of the complex error function. *SIAM J. Numer. Anal.*, 31(5):1497–1518, October 1994.

[13] Particle Data Group. Review of particle properties. *Phys. Rev. D*, 45, 1992.

[14] http://en.wikipedia.org/wiki/Bethe_formula. Last checked November 2014.

[15] B. Rossi. *High Energy Particles*. Prentice-Hall, Inc., Englewood Cliffs, NJ, 1st edition, 1952.

[16] W. Blum, W. Riegler, and L. Rolandi. *Particle Detection with Drift Chambers*. Springer, 2nd edition, 2008.

[17] H. Schindler, Garfield++ User Guide (Version 2014.1), http://cern.ch/garfieldpp, 2014.

[18] F. Cerutti, Beam Material Interaction, Heating and Activation. *Presentation at CAS on Accelerator Protection.*, November 2014.

[19] http://en.wikipedia.org/wiki/Charge_radius#History. Last checked November 2014.

[20] A. Fasso, et al., "FLUKA: a Multi-Particle Transport Code", CERN-2005-10, INFN/TC_05/11, SLAC-R-773, 2005.

[21] G. Battistoni, et al., "The FLUKA Code: Description and Benchmarking", Proceedings of the Hadronic Shower Simulation Workshop 2006 at Fermilab, Batavia, IL, USA, AIP Conference Proceeding, Vol. 896, p. 31–49, 2007.
[22] A. Lechner, B. Auchmann, T. Baer, F. Cerutti, V. Chetvertkova, B. Dehning, E. B. Holzer, O. Picha, M. Sapinski, N. V. Shetty, and E. Skordis. BLM thresholds for post-LS 1 LHC operation: UFOs and orbit bumps in the arcs and straight sections. Presentation at the Workshop on Beam-Induced Quenches, September 2014.
[23] T. Baer. *Very fast losses of the circulating LHC beam, their mitigation and machine protection.* PhD thesis, Universität Hamburg, 2013.
[24] A. Lechner. Private communication. November 2014.